Materials Research Proceedings 28 (2023) 1471-1480 https://doi.org/10.21741/9781644902479-159

Examination of intrinsic and extrinsic size effect in thin specimens through crystal plasticity frameworks

GÜNAY Enes[1,a], BULUT Orhun[1,b] and YALÇINKAYA Tuncay[1,c *]

[1]Department of Aerospace Engineering, Middle East Technical University, Ankara 06800, Türkiye

[a]enes.gunay@metu.edu.tr, [b]orhun.bulut@metu.edu.tr, [c]yalcinka@metu.edu.tr

Keywords: Crystal Plasticity, Size Effect, t/d Ratio Influence

Abstract. Manufacturing devices at the microscale requires a precise analysis for desirable mechanical behavior. As the products of microscale forming operations have a comparable thickness dimension with grain size, the ratio between thickness and grain size (t/d) becomes an important aspect of mechanical behavior. A number of experimental studies investigated this phenomenon and have shown the influence of the t/d ratio in micron-sized sheet specimens. On the other hand, the computational studies addressing this phenomenon employing micromechanics-based models are quite restricted. The current study aims to investigate the t/d ratio effect through finite element method (FEM) simulations with both local and nonlocal crystal plasticity frameworks. The numerical analyses with the local crystal plasticity framework are obtained by utilizing two different methodologies, where the initial slip resistance is taken as constant or modified using a subroutine based on grain size effects and slip system interactions (see [1]).

Introduction

Microelectromechanical systems are commonly used in different areas such as medicine, portable devices, and inertial measurement units. These systems are composed of micron-sized components that necessitate an investigation of their mechanical behavior. At such small scales, material behavior is heavily size dependent. The effect of grain boundaries and grain dimensions begin to dictate the material behavior (see [2]). However, when these specimens become so thin that there are very few grains in thickness direction, it is not enough to consider the grain size effects only (see [3]). Experiments in the literature have shown that the ratio of specimen thickness to average grain diameter is an important factor determining material response (see e.g. [4,5,6]). In these experiments, the t/d ratio is controlled by keeping one parameter (either specimen thickness or average grain diameter) constant while changing the other. The experiments show that the plasticity response from t/d parameter can be categorized in three main regions (see [5]). Very thin materials that lie in $t/d < 1$ region contain one or very few grains in the thickness direction. This results in a large majority of grains lying at the material surface and an independence of material response from the t/d ratio. Beyond this region, the number of grains in thickness direction begins to increase, yielding a multi-crystal behavior and rapid increase of stress response until the critical t/d ratio is achieved. The critical t/d ratio can be thought of as a material property. Upon reaching this value, the material begins to show proper polycrystalline behavior and acts as a bulk material. The influence of t/d ratio becomes insignificant since the surface grains are in very few numbers (see [7]).

In this paper, the behavior of such thin specimens is examined with three different approaches. First, a conventional local crystal plasticity is used. Local crystal plasticity frameworks do not have an intrinsic length scale parameter. Then, a lower order strain gradient crystal plasticity framework is implemented as an ABAQUS UMAT subroutine. Strain gradient methods have an intrinsic length scale parameter that allows them to predict size effects at the microscale (see e.g.

[8]). The higher order strain gradient formulations have higher order stresses which make them challenging to implement (see e.g. [9,10]). However, since the magnitude of the higher order stresses are often small, lower order approaches have also been used to obtain similar result except for boundary layers near interfaces or material surfaces as explained in [11]. The last method used is a subroutine that uses Hall-Petch theory to define initial slip resistance to crystals at each material point. This subroutine is implemented into the crystal plasticity framework. It is modified to work together with Voronoi tessellation geometries obtained from Neper program (see [12]). Grain misorientations and distance to grain boundaries at each point of the crystal structure is taken into account to provide a non-uniform distribution of initial slip resistance throughout the polycrystal specimens. Specimens with different thicknesses are simulated under uniaxial tension condition with all three methods and the results are discussed in detail.

The structure of this paper is as follows. First, the constitutive relations for both local and strain-gradient framework are described. Then, the material constants of aluminum alloy AA6016 in T4 temper condition, as well as the geometry parameters used in the finite element models are given. Additionally, the boundary conditions of the uniaxial tension are explained. Finally, the results are presented and compared with experimental findings in the literature.

Crystal Plasticity Frameworks

In the finite element analysis of the t/d effect, both a rate-dependent local, and a rate-dependent strain gradient crystal plasticity model is employed. This framework is based on a local crystal plasticity ABAQUS user material subroutine (UMAT) (see [13]). The UMAT subroutine is modified to include non-local strain-gradient effects using lower-order formulation following the theory of [10]. Since local crystal plasticity models do not inherently include size effects, it would not be possible to correctly predict the intrinsic size effect due to the change in grain size. The modification to include strain gradient effects in the constitutive formulations allows the size effects of crystal grains to be captured in simulations through geometrically necessary dislocations (GNDs).

The deformation gradient is decomposed into elastic and plastic components,

$$\mathbf{F}=\mathbf{F}^{e}\mathbf{F}^{p} \tag{1}$$

It is assumed that plastic deformation only occurs as a result of plastic slip. The elastic component of the deformation gradient only considers the stretching and rotation of the crystal lattice. The plastic component of the deformation gradient evolves according to the following flow rule

$$\dot{\mathbf{F}}^{p}=\mathbf{L}^{p}\mathbf{F}^{p} \tag{2}$$

where the plastic component of velocity gradient $\mathbf{L}^{p}$ is defined as the integration of plastic slip rate $\dot{\gamma}^{\alpha}$ on each slip system α that has slip direction and normal $\mathbf{m}^{\alpha}$ and $\mathbf{n}^{\alpha}$ respectively. The crystal plasticity framework consists of 12 active slip systems for a face-centered cubic material.

$$\mathbf{L}^{p}=\dot{\mathbf{F}}^{p}\mathbf{F}^{p-1}=\sum_{\alpha=1}^{N}\dot{\gamma}^{\alpha}\left(\mathbf{m}^{\alpha}\otimes\mathbf{n}^{\alpha}\right) \tag{3}$$

The slip rate is expressed in power law form, as,

$$\dot{\gamma}^{\alpha}=\dot{\gamma}_{0}\left|\frac{\tau^{\alpha}}{g_{T}^{\alpha}}\right|^{n}\operatorname{sign}(\tau^{\alpha}) \tag{4}$$

where $\dot{\gamma}_0$ is the reference slip rate, τ^α is the resolved shear stress, g_T^α is the total slip resistance, n is the rate sensitivity exponent, and $\mathrm{sign}(x)$ is the sign function. In this formulation, the total slip resistance is a combination of slip resistance caused by statistically stored dislocations (SSDs) and geometrically necessary dislocations (GNDs).

$$g_T^\alpha = \sqrt{{g_{ssd}^\alpha}^2 + {g_{gnd}^\alpha}^2} \tag{5}$$

The SSD slip resistance is described by the following relation,

$$\dot{g}_{ssd}^\alpha = \sum_{\beta=1}^{N} h^{\alpha\beta} \left|\dot{\gamma}^\beta\right| \tag{6}$$

From [14], the self and latent hardening law is expressed as,

$$h^{\alpha\alpha} = h_0 \, \mathrm{sech}^2 \left|\frac{h_0 \gamma}{g_s - g_0}\right| \tag{7}$$

$$h^{\alpha\beta} = q^{\alpha\beta} h^{\alpha\alpha} \tag{8}$$

where h_0 is the initial hardening modulus, g_s is the saturation slip resistance, g_0 is the initial slip resistance and $q^{\alpha\beta}$ is the latent hardening coefficient. The strain gradient framework assumes that there are no initial GNDs in the model, and GNDs only evolve because of strain gradient effects over time. Hence, the initial slip resistance is purely related to SSDs. The GND slip resistance is a formulation based on internal length scale parameter as well as the GND density of the crystals.

$$g_{gnd}^\alpha = g_0 \sqrt{l \eta_{gnd}^\alpha} \tag{9}$$

The length scale parameter l is defined as,

$$l = \frac{\alpha_T^2 \mu_s^2 b}{g_0^2} \tag{10}$$

Here, α_T is the Taylor coefficient that depends on the dislocation mechanisms of the crystal, μ_s is the shear modulus and b is the Burger's vector length. The GND density is described as,

$$\eta_{gnd}^\alpha = \left|\mathbf{n}^\alpha \times \sum_{\beta=1}^{N} \mathbf{m}^\alpha \mathbf{m}^\beta \nabla \gamma^\beta \times \mathbf{n}^\beta\right| \tag{11}$$

The calculation of strain gradient in a lower-order framework involves finite element operations. Using an 8-node 3D brick element with 8 Gauss integration points, the plastic slip values on each integration point is extrapolated to element nodes (see [15] for details). Then, a nodal averaging of the plastic slip is performed on nodes of neighboring elements. Finally, the gradient of strain is computed at the position of integration points.

Numerical Analysis

The numerical parameters of thickness/grain diameter ratio simulations are given in this section. A user material subroutine (UMAT) in the finite element software ABAQUS is used for crystal plasticity finite element method (CPFEM) simulations. The details of crystal plasticity parameters and the geometry-based initial slip resistance subroutine parameters are provided hereafter.

Using the material data of AA6016 in T4 temper condition from [16], the material parameters for the crystal plasticity framework are identified using a representative volume element (RVE) with 300 grains. This number of grains is sufficient to obtain an isotropic response from a polycrystal RVE in a reasonable computation time. The stress-strain response of the simulations is fitted to experimental material data under symmetric boundary conditions and tensile loading. Since the RVE is not morphologically periodic, symmetry boundary conditions are used to simulate the uniaxial tension at constant stress triaxiality of 0.33. Elastic stiffness coefficients for Al alloy are taken for cubic behavior from [17] as $C_{11} = 108.2$ GPa, $C_{12} = 61.3$ GPa, $C_{44} = 28.5$ GPa. Reference slip rate $\dot{\gamma}_0$ and the rate sensitivity exponent n are $10^{-3}\,s^{-1}$ and 20, respectively. The latent hardening parameter q is taken as 1.4. The hardening parameters are fitted using an RVE are initial hardening modulus h_0, saturation slip resistance g_s and initial slip resistance g_0, which are 190 MPa, 95 MPa and 47 MPa, respectively.

Table 1. Dimensions and total grains of the specimens used in simulations.

thickness [μm]	mean grain diameter [μm]	t/d ratio	Total number of grains	Number of finite elements	Avg. elements per grain
18	59	0.3	665	63368	95.3
35	73	0.48	665	62208	93.5
70	93	0.75	665	51076	76.8
105	105	1	703	50000	71.1
147	105	1.4	985	70000	71.0
189	105	1.8	1266	90000	71.1
211	105	2	1414	110000	77.8
253	105	2.4	1696	130000	76.7
295	105	2.8	1976	150000	75.9
316	105	3	2117	160000	75.6
358	105	3.4	2398	180000	75.1
400	105	3.8	2680	200000	74.6
484	105	4.6	3242	240000	74.0
526	105	5	3524	260000	73.8
568	105	5.4	3805	280000	73.6

The lower-order strain gradient theory requires an intrinsic length scale parameter for the slip resistance contribution of GNDs to be determined and the size effects to be predicted. The relation for the length scale parameter that governs the gradient effects is given in Eq. 10 (see [10]). The details of Taylor alpha coefficient can be found in [18]. In this problem, it is taken as 0.5. The shear modulus of AA6016 T4 is taken as 26 GPa and the Burger's vector magnitude is taken as 0.286 nm from [19]. The length scale parameter is calculated as 23.86 μm. However, above a certain element size in the FEM mesh, the lower-order model is mesh dependent. The GNDs are high in density in regions with non-uniform strain states such as grain boundaries. New dislocations must be introduced to obtain a homogenous plastic deformation in these regions (see [20]). If these regions are not modeled with an adequately fine mesh, strain gradients cannot be realized correctly. In this work, since there are many grains in the polycrystal structure, the computation times would be very long if a finer mesh was used. Hence, the length scale parameter is set to 500 μm after an element size sensitivity analysis to perform a qualitative comparison with the experiments.

A subroutine that calculates initial slip resistance based on the distance to grain boundaries on each integration point is implemented and tested in this work. This subroutine is built into the crystal plasticity framework and is only used to determine g_0. The details can be found in (see [1]). The size effects are realized in the initial slip resistance by the following relation,

$$g_0^{\alpha}=\tau_0+\frac{k^{\alpha}}{\sqrt{L^{\alpha}}} \tag{12}$$

where τ_0 is the critical resolved shear stress of a theoretically infinite crystal, taken as 0.05 MPa. L^{α} is the distance at a material point from grain boundaries in the direction of slip for a slip system. k^{α} is the micro Hall-Petch coefficient calculated as,

$$k^{\alpha}=K\left(1-m^{\alpha'}\right)^{c} \tag{13}$$

K and c are empirical coefficients, taken as 0.414 and 0.134, respectively. These values are obtained by fitting the stress-strain response using a 300 grain RVE with uniform 47 MPa initial slip resistance. $m^{\alpha'}$ is the Luster-Morris parameter for each slip system based on grain misorientation,

$$m^{\alpha'}=\left(\frac{\mathbf{m}_A^{\alpha}.\mathbf{m}_B^{\alpha}}{|\mathbf{m}_A^{\alpha}||\mathbf{m}_B^{\alpha}|}\right)\left(\frac{\mathbf{n}_A^{\alpha}.\mathbf{n}_B^{\alpha}}{|\mathbf{n}_A^{\alpha}||\mathbf{n}_B^{\alpha}|}\right) \tag{14}$$

where $\mathbf{m}^{\alpha}$ and $\mathbf{n}^{\alpha}$ are slip directions and normals respectively of each slip system α for grains A and B.

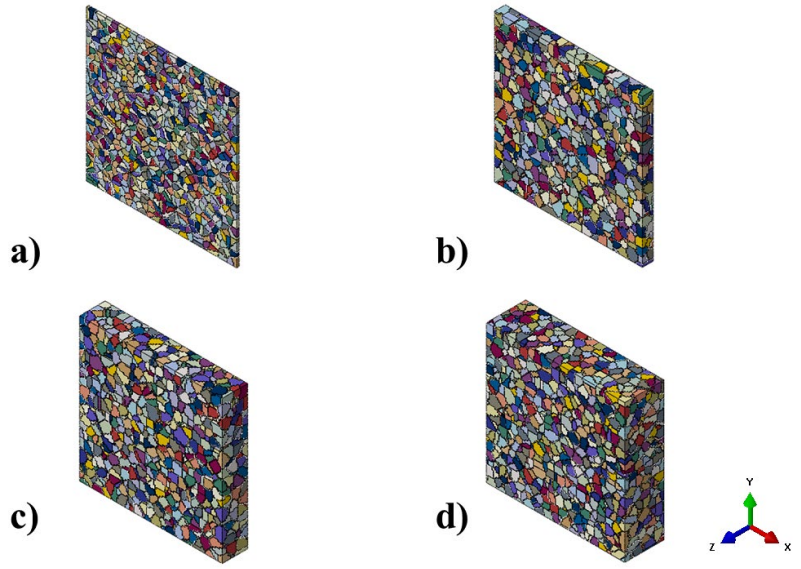

Fig. 1. Polycrystal microstructures of a) t/d = 0.48, b) t/d = 1.4, c) t/d =3, d) t/d = 5.4.

Tensile specimens of 2 mm x 2 mm x t mm thickness are generated through Neper software with dimensions given in Table 1. Examples of polycrystal structures at different t/d ratios are given in Fig. 1. Each grain is given a random crystal orientation. These orientations are random for each specimen with a different t/d ratio. However, they are kept constant while comparing local, strain-gradient, and geometry-based slip resistance simulations. 10% uniaxial tension is applied to each specimen in y-direction with a loading rate of $10^{-3}s^{-1}$ over 100 seconds.

Materials Research Proceedings 28 (2023) 1471-1480 https://doi.org/10.21741/9781644902479-159

Numerical Results

The numerical examples are presented in this section and a qualitative comparison with the experimental observations is conducted. Experimental results of true stress at 0.05 strain for a nickel polycrystal are represented in Fig. 2 from [5].

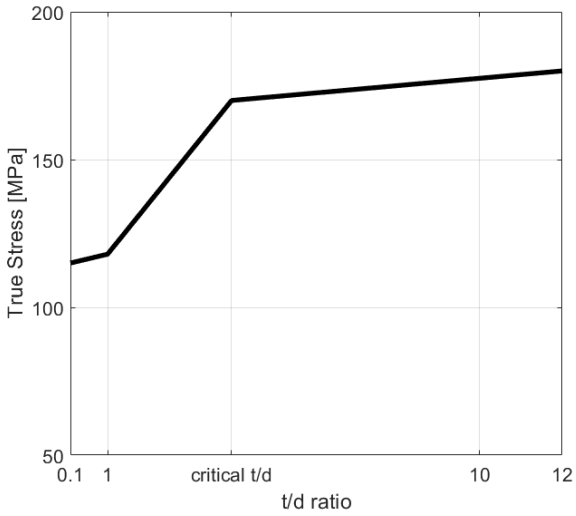

Fig. 2. Experimental values of true stress at 0.05 strain for different t/d ratios of Ni polycrystal (see [5]).

The FEM analysis results using the local crystal plasticity framework shows that, at low t/d ratio specimens (1 and below), the grains do not yield a stronger response despite their lower size compared to large t/d ratios. This is because the local crystal plasticity framework cannot predict intrinsic size effects. As a result, a monotonous increase in strength is observed in this region as seen in Fig. 3a. However, experimental results show that the stress response should not change significantly in t/d < 1 region. Without using a strain gradient framework or modifying the grains to have slip resistance based on their size and geometry, the increased strength of smaller grains cannot be reflected.

Finite element simulation results utilizing the strain gradient crystal plasticity framework are shown in Fig. 3b. The size-dependent solution shows that the strength of specimens in t/d < 1 range does not significantly change, similar to experimental findings. As specimen thickness decreases in this region, the average grain diameter also decreases. Hence, the material response gets stronger, and the significant stress increase in local solution due to surface grains and the presence of additional grains is no longer observed when the size effects are captured. Additionally, the critical t/d value is predicted as t/d = 3. In both Fig. 3a and 3b, a sharp, discontinuous increase can be seen between t/d = 1 and t/d = 1.4. This is a result of increased number of grains in the thickness direction. These grains allow for additional grain boundaries to be created, thus, a jump in stress response is observed.

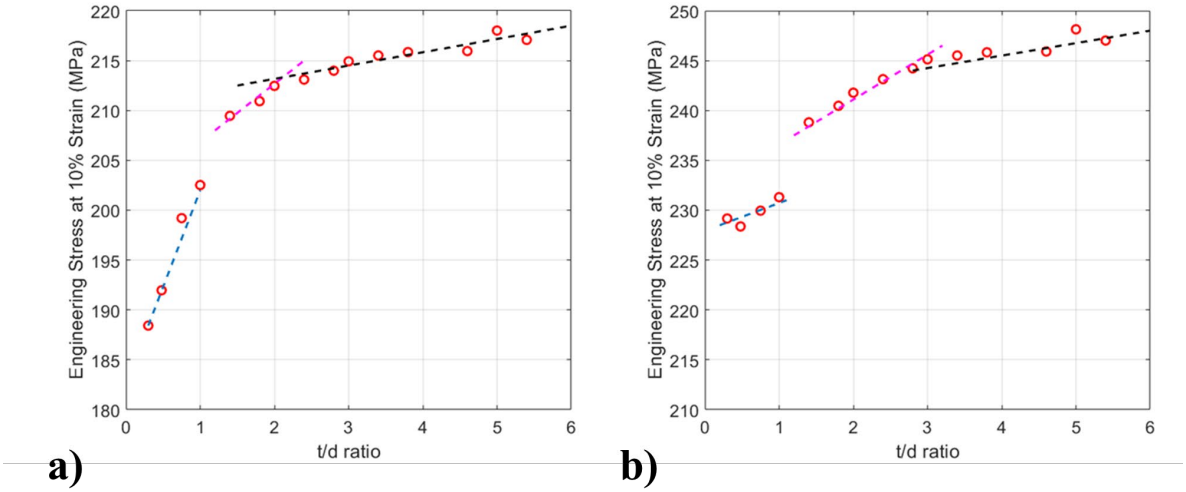

Fig. 3. Flow stress values of different t/d specimens at 10% strain with a) local crystal plasticity framework, b) strain gradient crystal plasticity framework.

After the critical t/d value is reached, the increase in stress response becomes less significant with increasing t/d values. This is in line with the experimental results. In the 1 < t/d < critical t/d region, there is a sharp increase in strength since additional grains in the thickness direction are now appearing and significantly increasing the material's strength. After the critical value, the thickness effect is no longer observed since the specimen approaches bulk size. There are enough grains in thickness direction so that newly formed grain boundaries do not impede dislocation motions significantly. The stress levels reached for every specimen is higher compared to results from local solution since GNDs impede deformation by increasing the slip resistance at locations where their densities are high.

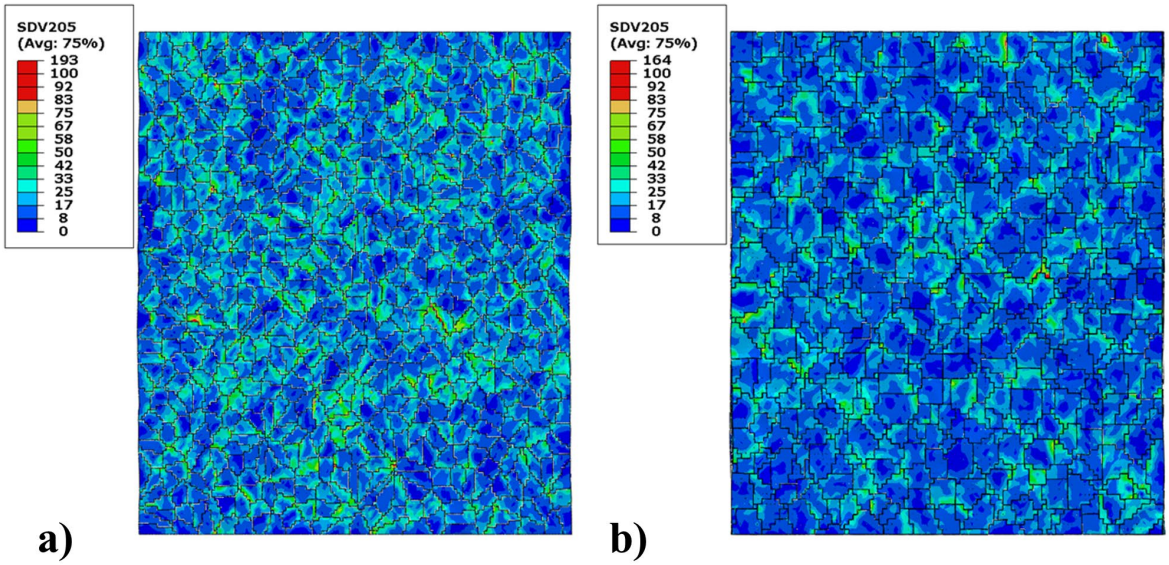

Fig. 4. GND densities [1/mm] of a) t/d = 0.48 and b) t/d = 5.4.

The GND densities of specimens having t/d ratios of 0.48 and 5.4 are presented in Fig. 4. Here, GND densities for each grain are highest at the grain boundaries. Neighboring grains with significant misorientation between each other can be spotted since GND densities would

concentrate at those locations. The density of GNDs is higher in the specimen with smaller t/d ratio, resulting in a higher slip resistance due to smaller grain sizes.

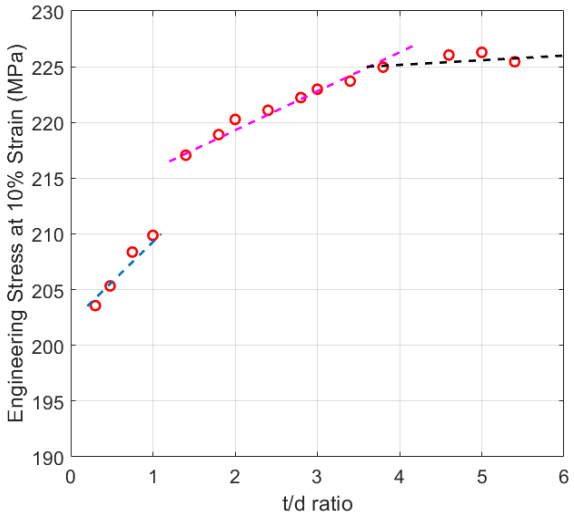

Fig. 5. Flow stress values of different t/d specimens at 10% strain with geometry-based initial slip resistance simulations.

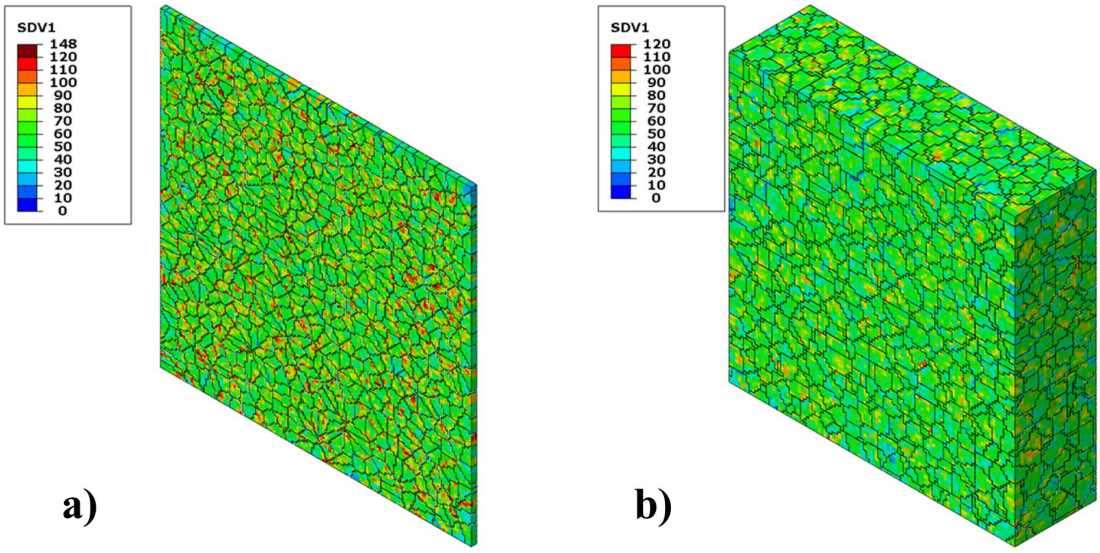

Fig 6. Comparison of initial slip resistance [MPa] at a) t/d = 0.48 and b) t/d = 5.4 for slip system (111)[0$\bar{1}$1].

Finally, the results of simulations where a geometry-based initial slip resistance is used are shown in Fig. 5. The critical t/d value is predicted higher with this method as approximately 4. Since the distance to grain boundaries is a parameter that determines the initial slip resistance at each material point, size effects are taken into account. At t/d < 1, an increase in strength can still be observed with increasing t/d, although at a much lower rate than the local solution. Moreover, after the critical t/d value, the strength increase slows down as expected from the experimental findings. Fig. 6 shows the comparison of initial slip resistance at t/d ratios 0.48 and 5.4 for one of the slip systems. There is a larger initial resistance assigned to elements in $t/d = 0.48$ on average since the grains are smaller and the integration points are closer to grain boundaries as a result.

Summary

In this work, a series of crystal plasticity finite element method simulations are conducted to examine the uniaxial tension loading responses of micron-sized specimens. Three different approaches have been used to obtain these results. Local crystal plasticity frameworks yield size-independent results since there is no information regarding grain or specimen size in their constitutive relations. A subroutine is utilized in a local framework to determine the initial slip resistance of crystals at every material point through a size-dependent approach. While this method does not influence constitutive relations, it is still able to capture the effects seen in experiments since smaller grains in low t/d ratios have their slip resistance increased compared to larger grains. The last method used is the lower-order strain-gradient framework. With this method, the density of GNDs is calculated and used in the constitutive relations directly based on a length scale parameter.

The results show that by using a strain-gradient framework or employing Hall-Petch theory to determine initial slip resistance of crystals, a similar trend to experimental findings in t/d<1 region can be found. As the thickness and t/d ratios of the specimens increase, an increase in their stress/strain response can be seen in every result case. This is attributed to the fact that new grain boundaries and more grains in the thickness direction are developing rapidly. Once the critical t/d value is reached, a different value is obtained with every method. The simulations using local crystal plasticity framework show that the critical t/d is obtained at 2. With the strain gradient framework, the critical value is found as 3. This indicates that there is still a considerable size dependence until this point. On the other hand, when Hall-Petch theory is utilized, the specimens reach this critical value and start showing bulk-material behavior at a t/d value of 4. This is consistent with the trends obtained from experiments as seen in Fig. 2. Additionally, the stress increase in the post-critical region is predicted slightly less in this case.

References

[1] D. Agius, A. Kareer, A. Al Mamun, C. Truman, D.M. Collins, M. Mostafavi, D. Knowles, A crystal plasticity model that accounts for grain size effects and slip system interactions on the deformation of austenitic stainless steels, Int. J. Plast. 152 (2022) 103249. https://doi.org/10.1016/j.ijplas.2022.103249

[2] T. Yalçinkaya, İ. Özdemir, I. Simonovski, Micromechanical modeling of intrinsic and specimen size effects in microforming, Int. J. Mater. Form. 11 (2018) 729-741. https://doi.org/10.1007/s12289-017-1390-3

[3] H.S. Kim, Y.S. Lee, Size dependence of flow stress and plastic behaviour in microforming of polycrystalline metallic materials, Proc. Inst. Mech. Eng., Part C: J. Mech. Eng. Sci. 226 (2012) 403-412. https://doi.org/10.1177/0954406211414473

[4] P.J.M. Janssen, T.H. De Keijser, M.G.D. Geers, An experimental assessment of grain size effects in the uniaxial straining of thin Al sheet with a few grains across the thickness, Mater. Sci. Eng. A 419 (2006) 238-248. https://doi.org/10.1016/j.msea.2005.12.029

[5] E. Hug, C. Keller, Intrinsic effects due to the reduction of thickness on the mechanical behavior of nickel polycrystals, Metall. Mater. Trans. A 41 (2010) 2498-2506. https://doi.org/10.1007/s11661-010-0286-3

[6] C. Keller, E. Hug, R. Retoux, X. Feaugas, TEM study of dislocation patterns in near-surface and core regions of deformed nickel polycrystals with few grains across the cross section, Mech. Mater. 42 (2010) 44-54. https://doi.org/10.1016/j.mechmat.2009.09.002

[7] O. Bulut, S.S. Acar, T. Yalçinkaya, The influence of thickness/grain size ratio in microforming through crystal plasticity, Procedia Struct. Integrity 35 (2022) 228-236. https://doi.org/10.1016/j.prostr.2021.12.069

[8] T. Yalçinkaya, Strain gradient crystal plasticity: Thermodynamics and implementation, in: G. Z. Voyiadjis (Eds.), Handbook of Nonlocal Continuum Mechanics for Materials and Structures, Springer, London/Berlin, 2017, pp.1001-1033.
[9] T. Yalçinkaya, İ. Özdemir, A.O. Firat, Inter-granular cracking through strain gradient crystal plasticity and cohesive zone modeling approaches, Theor. Appl. Fract. Mech. 103 (2019) 102306. https://doi.org/10.1016/j.tafmec.2019.102306
[10] T. Yalçinkaya, İ.T. Tandoğan, İ. Özdemir, Void growth based inter-granular ductile fracture in strain gradient polycrystalline plasticity, Int. J. Plast. 147 (2021) 103123. https://doi.org/10.1016/j.ijplas.2021.103123
[11] C.S. Han, H. Gao, Y. Huang, W.D. Nix, Mechanism-based strain gradient crystal plasticity-I, Theory, J. Mech. Phys. Solids 53 (2005) 1188-1203. https://doi.org/10.1016/j.jmps.2004.08.008
[12] R. Quey, P. Dawson, F. Barbe, Large-scale 3D random polycrystals for the finite element method: Generation, meshing and remeshing, Comput. Methods Appl. Mech. Eng. 200 (2011) 1729–1745. https://doi.org/10.1016/j.cma.2011.01.002
[13] Y. Huang, A user-material subroutine incorporating single crystal plasticity in the ABAQUS finite element program, Mech. Report 178 (1991)
[14] D. Peirce, R.J. Asaro, A. Needleman, An analysis of nonuniform and localized deformation in ductile single crystals, Acta Metall. 30 (1982) 1087–1119. https://doi.org/10.1016/0001-6160(82)90005-0
[15] E.P. Busso, F.T. Meissonnier, N.P. O'dowd, Gradient-dependent deformation of two-phase single crystals, J. Mech. Phys. Solids 48 (2000) 2333-2361. https://doi.org/10.1016/S0022-5096(00)00006-5
[16] H. Granum, V. Aune, T. Børvik, O.S. Hopperstad, Effect of heat-treatment on the structural response of blast-loaded aluminium plates with pre-cut slits, Int. J. Impact Eng. 132 (2019) 103306. https://doi.org/10.1016/j.ijimpeng.2019.05.020
[17]E. Nakamachi, C. Xie, H. Morimoto, K. Morita, N. Yokoyama, Formability assessment of FCC aluminum alloy sheet by using elastic crystalline viscoplastic finite element analysis, Int. J. Plast. 18 (2002) 617–632. https://doi.org/10.1016/S0749-6419(01)00052-3
[18] H. Mughrabi, The α-factor in the Taylor flow-stress law in monotonic, cyclic and quasi-stationary deformations: Dependence on slip mode, dislocation arrangement and density, Curr. Opin. Solid State Mater. Sci. 20 (2016) 411-420. https://doi.org/10.1016/j.cossms.2016.07.001
[19] O. Engler, C.D. Marioara, Y. Aruga, M. Kozuka, O.R. Myhr, Effect of natural ageing or pre-ageing on the evolution of precipitate structure and strength during age hardening of Al–Mg–Si alloy AA 6016, Mater. Sci. Eng. A 759 (2019) 520-529. https://doi.org/10.1016/j.msea.2019.05.073
[20] A. Arsenlis, D.M. Parks, Crystallographic aspects of geometrically-necessary and statistically-stored dislocation density, Acta Mater. 47 (1999) 1597-1611. https://doi.org/10.1016/S1359-6454(99)00020-8